Experimental Optimization of PLC-Integrated Multi-Loop PID Control for a Three-Level Electro-Hydraulic Elevator Using PSO and Cheetah Optimizer

Maryam Ali Karim
Department of Mechatronics Engineering, Al-Khwarizmi College of Engineering, University of Baghdad, Baghdad, Iraq
mariam.ali1301@kecbu.uobaghdad.edu.iq (corresponding author)

Maher Yahya Salloom
Department of Mechatronics Engineering, Al-Khwarizmi College of Engineering, University of Baghdad, Baghdad, Iraq
drmahir@kecbu.uobaghdad.edu.iq

Yasar N. Lafta
Department of Mechatronics Engineering, Al-Khwarizmi College of Engineering, University of Baghdad, Baghdad, Iraq
yasar@kecbu.uobaghdad.edu.iq

Received: 23 December 2025 | Revised: 15 January 2026, 4 February 2026, and 11 February 2026 | Accepted: 13 February 2026

Licensed under a CC-BY 4.0 license | Copyright (c) by the authors | *DOI: https://doi.org/10.48084/etasr.17143*

ABSTRACT

This study presents the design, modeling, and experimental evaluation of a three-level electro-hydraulic elevator system controlled by a Delta DVP-20SX2 Programmable Logic Controller (PLC) equipped with an integrated Proportional–Integral–Derivative (PID) module. The PLC, programmed in Ladder Logic using ISPSoft 2.46, regulates cabin motion across all three levels. A detailed MATLAB/Simulink model was developed, incorporating three PID controllers: one for displacement regulation via a proportional directional control valve and two for dynamic pressure regulation using a proportional pressure relief valve. Conventional PID parameters were initially tuned using the trial-and-error method based on time-domain performance indices and subsequently optimized using Particle Swarm Optimization (PSO) and the Cheetah Optimizer (CO). The optimized controllers are referred to as PSO-PID and CO-PID, respectively. The error standard used for the electro-hydraulic elevator control system is the Integral Time-weighted Absolute Error (ITAE) type. This study addresses the need to improve dynamic performance and control accuracy in electro-hydraulic elevator systems under maximum load conditions. Experimental results obtained under a 30 kg load for the displacement response showed that PSO-PID reduced rise time by 36.8% and settling time by approximately 37.2% while improving steady-state accuracy by nearly 80% compared with the conventional PID. The CO-PID controller further improved performance, achieving additional reductions of 13.6% in rise time and 13.8% in settling time relative to PSO-PID, as well as decreasing steady-state error by 37.5%. Overall, CO-PID achieved substantial reductions in rise and settling times (up to 45.4% and 45.7%, respectively) and improved steady-state accuracy by nearly 87% compared with the traditional PID. In pressure control loops, PSO-PID reduced settling time by up to 12.8%, whereas CO-PID achieved up to 16.4% faster stabilization relative to the conventional PID. The experimental results were in agreement with the developed MATLAB/Simulink model, confirming the high accuracy of the simulation in representing the system dynamics. These findings demonstrate the superior responsiveness, stability, and efficiency of the CO-PID controller for electro-hydraulic elevator applications.

Keywords-electro-hydraulic elevator; PID controller; PLC; Particle Swarm Optimization (PSO); Cheetah Optimizer (CO)

I. INTRODUCTION

Electro-hydraulic elevators are common in medium-rise buildings, especially in Northern Europe. They are favored for their low cost and simple mechanical design. Conventional hydraulic elevator systems typically employ a bottom-mounted piston and cylinder mechanism to lift and lower the cabin. These elevators often face reduced efficiency because of traditional throttle-based control methods. Performance improvements can be achieved by reducing response time, reducing vibration, and enhancing positioning accuracy, which leads to better reliability, passenger comfort, and energy efficiency [1]. Since the 1980s, significant advancements in electro-hydraulic control techniques have contributed to notable improvements in elevator performance, safety, and operational reliability [2]. Early studies have shown that enhancing control strategies can improve efficiency, increase performance accuracy, and achieve smoother operation in hydraulic elevator systems [3].

Several control strategies have been proposed for controlling the speed of hydraulic elevators, including Proportional–Integral–Derivative (PID) controllers and self-tuning fuzzy PID controllers. Authors in [4] designed, modeled, and simulated both controllers using MATLAB/Simulink and their results showed that the self-tuning fuzzy PID controller outperformed the conventional PID. Authors in [5] investigated an electro-hydraulic servo system that combines a proportional valve with a PI controller to control speed in hydraulic elevators. Experimental testing demonstrated quicker response times and reduced vibration. In a related study, authors in [6] proposed a practical, indirect hydraulic elevator based on a position sensor and controlled by a variable-speed pump. The results demonstrated high positioning accuracy and smooth operation.

As demonstrated in [7], a three-story elevator with a telescopic cylinder under a Programmable Logic Controller (PLC) control achieved precise speed and position regulation through modeling and simulation. Authors in [3] implemented a variable voltage/variable frequency control system using a PID controller to improve elevator speed. A control system model was built in MATLAB/Simulink and then tested experimentally through up-and-down motion trials, showing good agreement between simulation and experiment. Authors in [8] developed an experimental electro-hydraulic elevator model by integrating a PLC with a proportional valve to achieve precise and efficient cabin movement. The results demonstrated smooth cabin movement and excellent control. In a related study, a P-Q electro-hydraulic proportional valve was used for pressure and flow control of a hydraulic elevator system, and the model was computer-simulated, achieving high control accuracy and smooth operation [9].

Authors in [10] simulated a three-stage telescopic cylinder in MATLAB/Simulink and verified safe operation with minimal vibration. Authors in [11] presented a performance comparison of different PLCs integrated with PID controllers for controlling proportional valves and hydraulic cylinders, which showed increased system stability and reduced settling time. In a separate study, authors in [12] practically implemented an elevator model based on a PLC, a DC motor, and sensors, resulting in improved reliability and passenger comfort. Authors in [13] demonstrated through practical application that PLC-controlled proportional valves outperform conventional valves in terms of response, smoothness, and energy usage.

In another study, authors in [14] implemented a practical PLC/Human–Machine Interface (HMI)-based control for a hydraulic elevator using a directional valve and hydraulic motor, improving operational stability. Simulation of an electro-hydraulic conveyor system using proportional control in MATLAB showed that a PID controller, with parameters initially set by trial and error and subsequently optimized, improved overall system performance [15]. Authors in [16] developed an electro-hydraulic elevator prototype controlled via PID and a proportional valve with Arduino-DAQ automation, achieving significant performance improvement. In a different study, stable flow control was demonstrated using a PLC-based PID tuned with Ziegler-Nichols rules [17]. Authors in [18] reviewed the practical application of proportional electro-hydraulic systems controlled by a PLC, demonstrating precise regulation of cylinder speed and position, as well as stability under varying loads.

Authors in [19] simulated an electro-hydraulic system model using MATLAB/Simulink and applied a PID controller, adjusting its parameters using the Ziegler-Nichols method. The simulation results showed system stability and improved performance, which was verified experimentally. Authors in [20] investigated the experimental use of a digital hydraulic valve controlled by a PLC and servo motors, showing improved control of variable-speed hydraulic systems. Authors in [21] simulated an electro-hydraulic system using MATLAB and employed the Improved Differential Evolution (IDE) algorithm to optimize PID parameters, achieving greater motion tracking accuracy and system stability compared with conventional PID controllers.

Although many studies have examined the use of PID controllers in hydraulic elevator systems, most still rely on fixed or conventionally tuned PID gains, focusing on simulation-based control and providing only limited improvements in speed and positioning accuracy. Recent studies have introduced advanced approaches such as variable-speed pumps, proportional valves, and improved PID optimization techniques, but few have applied these optimizations to real systems, leaving a gap between simulated and actual performance.

This research addresses this gap by transferring PID gains obtained from MATLAB/Simulink directly to a practical PLC-based electro-hydraulic elevator model, representing a novel approach compared with previous studies. Furthermore, this work introduces the Cheetah Optimizer (CO) as a novel method for PID tuning in electro-hydraulic elevators, and its performance is evaluated alongside the widely used Particle Swarm Optimization (PSO) algorithm. A three-story electro-hydraulic elevator system with integrated PID units and a PLC was developed, incorporating both displacement and pressure control to ensure precise and consistent system performance. Conventional PID values were first applied to establish

baseline performance, after which optimized values derived from PSO and CO were implemented, resulting in improved positioning accuracy, reduced settling time, and enhanced system stability under varying operating conditions.

II. THEORETICAL ANALYSIS

This section presents the overall structure of the hydraulic system. Figures 1 and 2 illustrate the closed-loop control for displacement and pressure using the proportional directional valve and the proportional pressure relief valve with PID controllers.

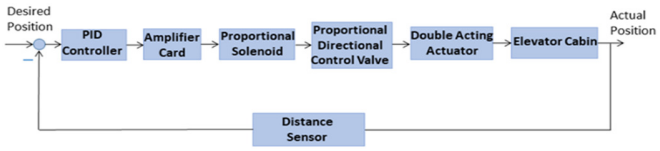

Fig. 1. Electro-hydraulic elevator system with displacement control loop.

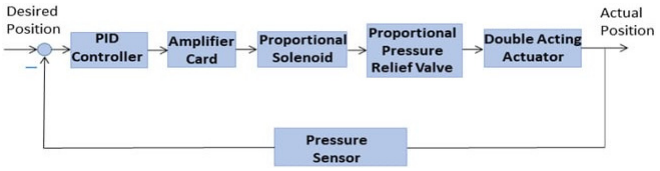

Fig. 2. Electro-hydraulic elevator system with dual pressure control loop.

In this study, the electro-hydraulic elevator was modeled in MATLAB/Simulink using two complementary approaches. The first approach involved formulating a dynamic mathematical model derived from fundamental physical equations, which enabled the verification of the system's performance and control strategy. The second approach involved using physical blocks available in Simulink libraries to practically represent physical behavior. Both approaches together provided theoretical verification and practical application of the proposed system.

A. Equation-Based Simulink Model

1) Double-Acting Hydraulic Cylinder

In a hydraulic elevator, the actuator is represented by a double-acting hydraulic cylinder that converts hydraulic power defined by pressure and flow into mechanical motion to raise and lower the cabin. The flow behavior in the cylinder is described by the following equation [22]:

$$Q_{in} = K\frac{dP_L}{dt} + A\dot{x} + \frac{P_L}{R_{lkga}} \quad (1)$$

where Q_{in} is the total inflow rate delivered to the hydraulic actuator in ($m^3 \cdot s^{-1}$), $K = V_t/\beta_e$ is the compressibility coefficient in ($m^3 \cdot Pa^{-1}$), V_t is the total control volume of the cylinder chambers and pipelines, β_e is the effective bulk modulus of the fluid including entrapped air effects , $\frac{dP_L}{dt}$ is the flow component arising from the compressibility of the hydraulic fluid in ($Pa \cdot s^{-1}$), $A\dot{x}$ is the volumetric flow rate required to produce piston (cylinder) motion in ($m^3 \cdot s^{-1}$), and $\frac{P_L}{R_{lkga}}$ is the leakage flow through the cylinder's internal clearances in ($m^3 \cdot s^{-1}$); P_L is the load pressure in the cylinder in (Pa); and R_{lkga} represents the internal leakage resistance of the hydraulic cylinder. Rearrangement of (1) yields the following expression for the actuator load pressure:

$$P_L = \frac{1}{K}\int\left(Q_{in} - A\dot{x} - \frac{P_L}{R_{lkga}}\right)dt \quad (2)$$

This equation describes the way in which the actuator's internal pressure responds to the input flow, leakage losses, and piston motion. Following [23], the actuator's force equilibrium equation can be expressed as:

$$P_L\, A = F_L + m\ddot{x} + \beta\dot{x} + K_1 x \quad (3)$$

where P_L is the internal pressure of the cylinder in (Pa); A denotes the piston area; F_L indicates the external load acting on the actuator; m denotes the moving equivalent mass in (kg); $\ddot{x}$ represents the piston acceleration in ($m \cdot s^{-2}$); β denotes the viscous damping coefficient between the piston and the hydraulic fluid in ($N \cdot s \cdot m^{-1}$); $\dot{x}$ represents the piston velocity in ($m \cdot s^{-1}$); K_1 is the stiffness coefficient of the cylinder in ($N \cdot m^{-1}$); and x denotes the piston displacement in (m).

Figure 3 illustrates the application of the hydraulic cylinder dynamics equations in the Simulink model.

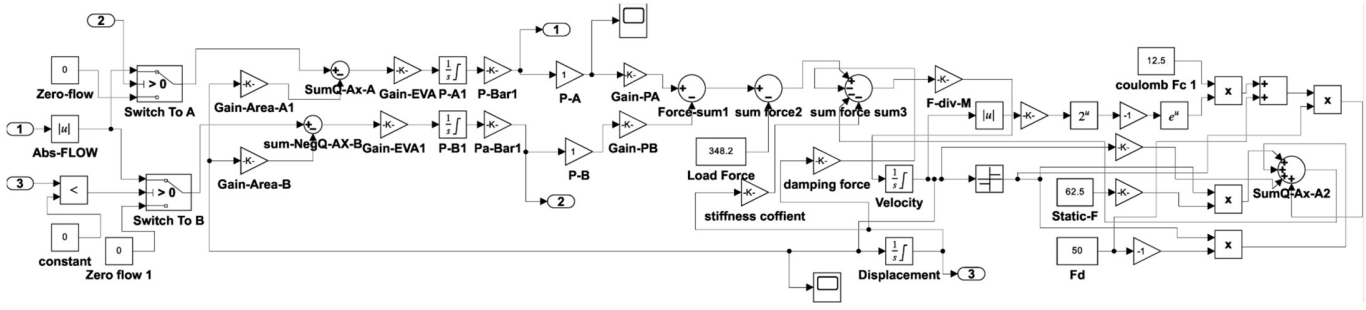

Fig. 3. Dynamic representation of the hydraulic cylinder in Simulink.

2) Proportional Hydraulic Directional Valve

This dynamic model of the valve spool is formulated based on Newton's second law [24]:

$$m\ddot{x} = \Delta PA - Kx - C\dot{x} \quad (4)$$

Here, m denotes the mass of the spool in (kg); $\ddot{x}$ denotes the spool linear acceleration in ($m \cdot s^{-2}$); ΔP is the pressure

difference across the spool in (pa); A represents the effective area of the spool in (m^2); K is the spring constant of the spool in ($N \cdot m^{-1}$); x represents the displacement of the spool in (m); whereas $C\dot{x}$ corresponds to the viscous damping force (damping coefficient in $N \cdot s \cdot m^{-1}$ times velocity in $m \cdot s^{-1}$).

$$Q = C_d A_v \sqrt{\frac{2\Delta P}{\rho}} \quad (5)$$

Here, Q denotes the volumetric flow rate ($m^3 \cdot s^{-1}$); C_d denotes discharge coefficient; A_v represents the effective orifice area (m^2), which is directly related to the spool displacement; ΔP corresponds to the pressure drop across the valve (Pa); and ρ is the density of the hydraulic fluid ($kg \cdot m^{-3}$). The dynamic equations for the proportional directional control valve are represented by Simulink as shown in Figure 4.

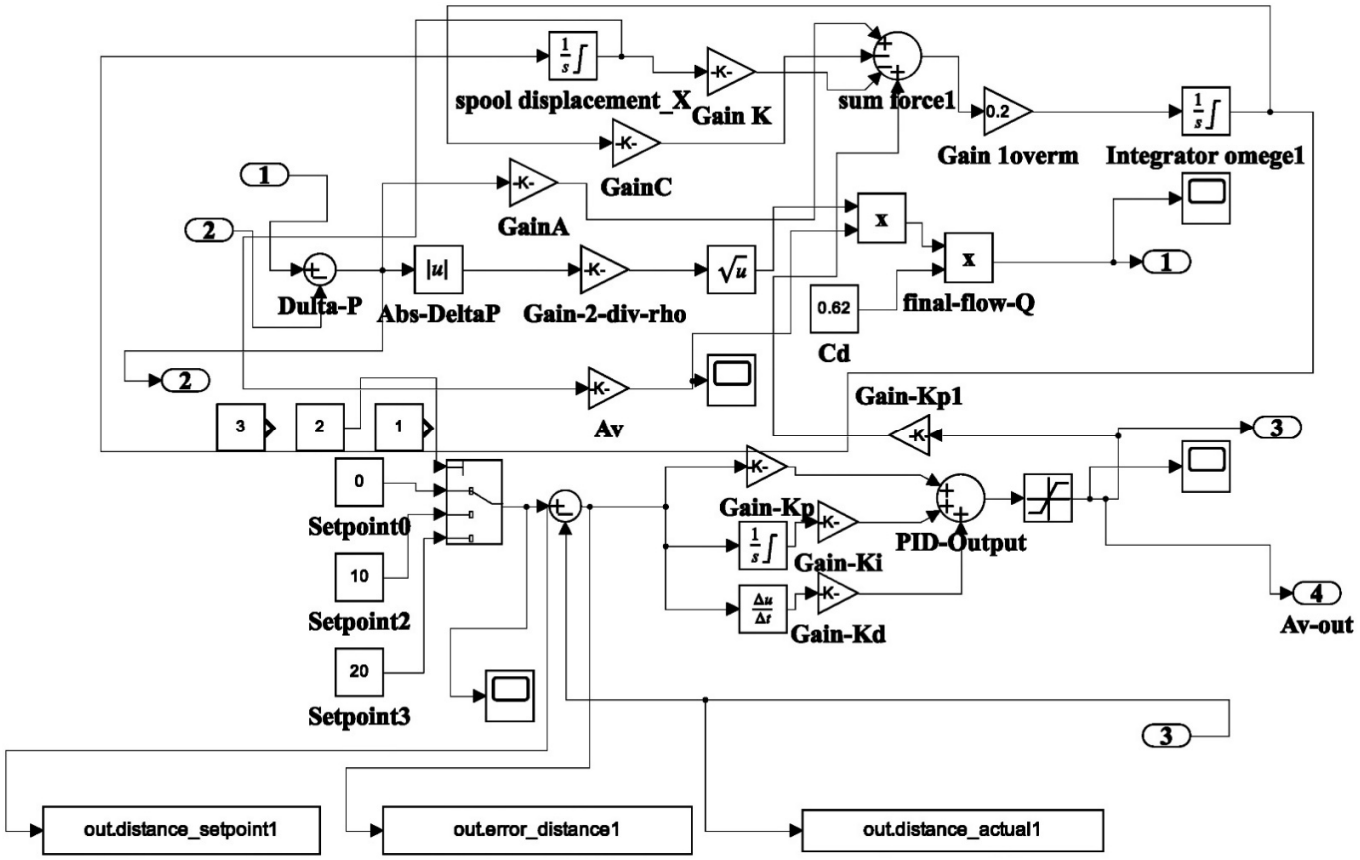

Fig. 4. Dynamic equations of the proportional valve with PID displacement in the Simulink model.

3) Proportional Pressure Relief Valve

As stated in [23], the valve spool dynamic behavior can be described by the following equation:

$$m\ddot{x} + C\dot{x} + Kx + F_s = \Delta PA \quad (6)$$

where m denotes the mass of the spool in (kg); $\ddot{x}$ is the spool linear acceleration in ($m \cdot s^{-2}$); ΔPA is the hydraulic force acting on the spool ($Pa \cdot m^2 = N$); C is the viscous damping coefficient of the spool in ($N \cdot s \cdot m^{-1}$); $\dot{x}$ represents the linear velocity of the spool in ($m \cdot s^{-1}$); K denotes the spring constant of the spool in ($N \cdot m^{-1}$); x is the displacement of the spool in (m); F_s is the pre-compression spring force acting on the spool in (N).

Figure 5 shows the Simulink model of the dynamic equations for a proportional pressure relief valve, with input values of the desired and actual pressures represented and connected to the valve.

4) Fixed-Displacement Gear Pump

The operation of a fixed-displacement pump is described by the following equation [23]:

$$q = D\omega - K_{leak}\Delta P \quad (7)$$

where q denotes the volumetric flow rate ($m^3 \cdot s^{-1}$), D is the pump displacement per radian ($m^3 \cdot rad^{-1}$), ω is the angular velocity ($rad \cdot s^{-1}$), K_{leak} is the leakage coefficient ($m^3 \cdot s^{-1} \cdot Pa^{-1}$), and ΔP represents the pressure rise across the pump (Pa).

$$T = \frac{\Delta P D_p}{\eta_{mech}} \quad (8)$$

where T indicates the torque at the pump shaft (N·m); ΔP is the pressure difference between the pump inlet and outlet in (Pa); D_p is the pumps displacement per revolution ($m^3 \cdot rev^{-1}$); and η_{mech} is the mechanical efficiency.

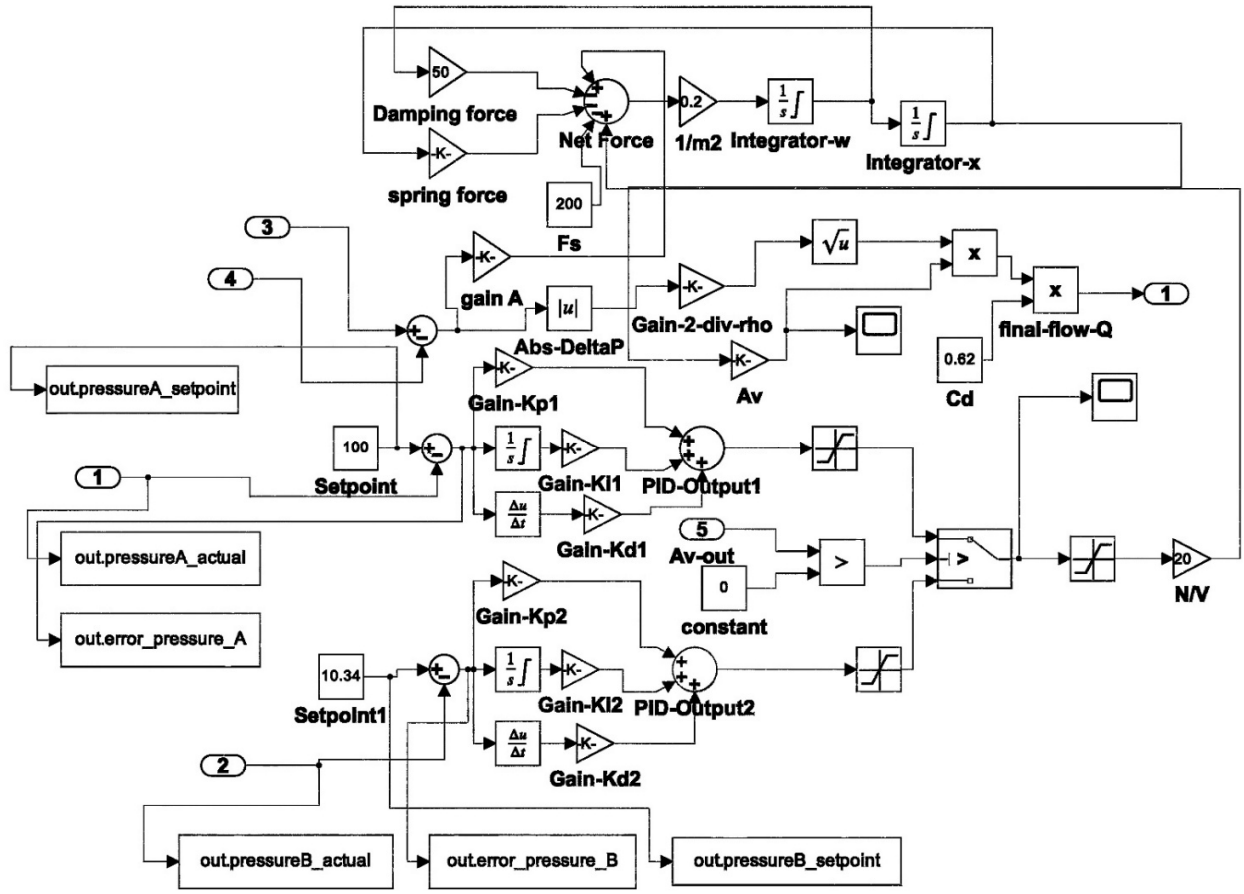

Fig. 5. Dynamic equation of the proportional pressure relief valve with dual PID pressure switching mechanism in the Simulink model.

$$K_{leak} = \frac{K_{HP}}{v \cdot \rho} \quad (9)$$

Here, K_{leak} is the hydraulic leakage coefficient in ($m^3 \cdot s^{-1} \cdot Pa^{-1}$); K_{HP} denotes the Hagen–Poiseuille coefficient; v is the kinematic viscosity of the fluid ($m^2 \cdot s^{-1}$); and ρ represents the fluid density ($kg \cdot m^{-3}$).

$$K_{HP} = \frac{D \cdot \omega_{nom}(1 - \eta_v) \cdot \rho_{nom} \cdot v_{nom}}{P_{nom}} \quad (10)$$

In this relation, K_{HP} denotes the Hagen–Poiseuille coefficient; D represents the pump displacement ($m^3 \cdot rev^{-1}$); ω_{nom} is the nominal angular velocity of the pump ($rad \cdot s^{-1}$); η_v denotes the mechanical efficiency; v_{nom} denotes the nominal kinematic viscosity of the fluid ($m^2 \cdot s^{-1}$); ρ_{nom} is the nominal density of the fluid ($kg \cdot m^{-3}$); and P_{nom} corresponds to the nominal pressure (Pa).

$$\Delta P = P_P - P_T \quad (11)$$

Here, ΔP indicates the differential pressure acting over the pump (Pa); whereas P_P and P_T correspond to the outlet and inlet gauge pressures of the pump, respectively.

The Hagen-Poiseuille principle [23] is applied to calculate the leakage flow under the assumption that it varies linearly with the pressure difference across the pump:

$$\Delta P = \left(\frac{128\,\mu}{\pi d^4}\right) q_{leak} \quad (12)$$

Here, ΔP is the pressure difference across the pump (Pa); q_{leak} denotes the leakage flow rate ($m^3 \cdot s^{-1}$); μ is the dynamic viscosity of the hydraulic fluid (Pa·s); and d represents the diameter of the leakage passage (m).

Because manufacturers' datasheets typically do not specify the mechanical performance of pumps, it is commonly approximated using the ratio between overall efficiency and volumetric efficiency, assuming hydraulic losses can be disregarded:

$$\eta_m = \frac{\eta_t}{\eta_v} \quad (13)$$

Here, η_m represents the mechanical efficiency; η_t denotes the overall efficiency; and η_v corresponds to the volumetric efficiency. The hydraulic output power generated by the pump can be expressed as:

$$P_h = Q_a \cdot \Delta P \quad (14)$$

where P_h is the hydraulic power (W); Q_a indicates the actual flow rate ($m^3 \cdot s^{-1}$); and ΔP refers to the discharge pressure (Pa).

These equations were represented by Simulink as shown in Figure 6.

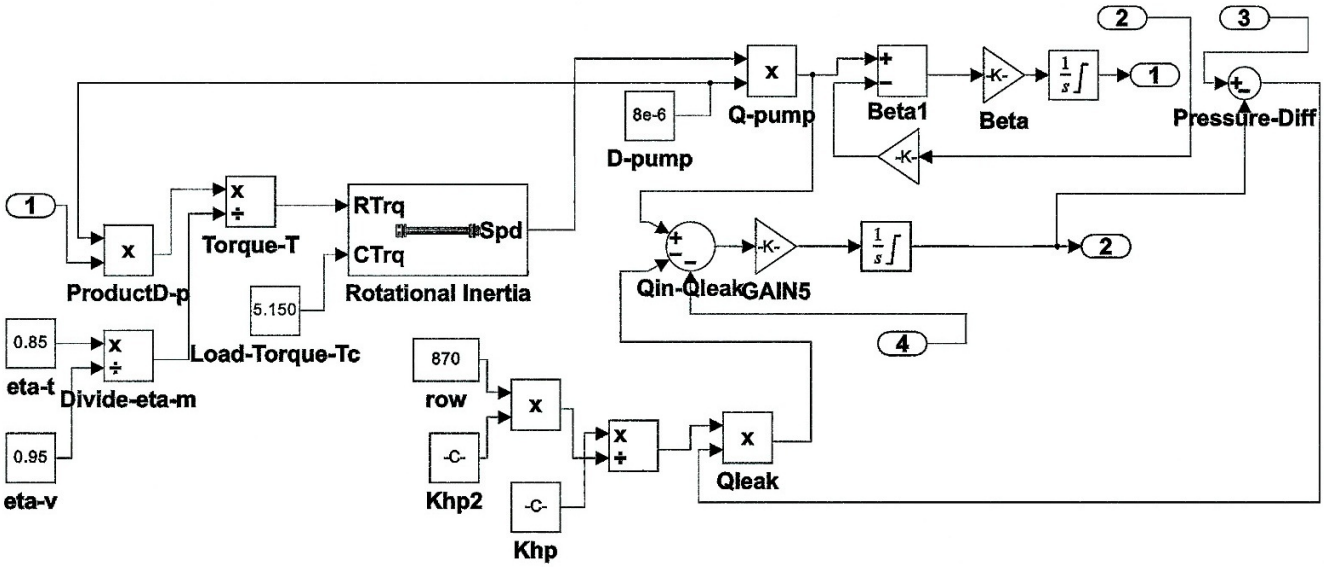

Fig. 6. Simulink model of the pump and motor.

All the mathematical equations derived for the electro-hydraulic elevator system were implemented using basic Simulink blocks, including PID controllers, Gain, Sum, and Switch blocks, as well as sensors for measuring pressure and displacement. The PID units were set to appropriate values for P, I, D, and signal limits to ensure precise control. Gain and Sum blocks were used to calculate and amplify the error signal, whereas Switch blocks selected the appropriate control signal based on the elevator's direction of movement. Pressure and displacement sensors with appropriate ranges for the hydraulic elevator system were also included, along with a simulation downtime of 10 s. The system was organized into clear subsystems to provide a complete and readable representation of the model. Each equation was expressed separately and then integrated within a single unified structure in order to simulate the physical behavior of each component of the system. Figure 7 illustrates the complete dynamic model, showing how all equations are combined.

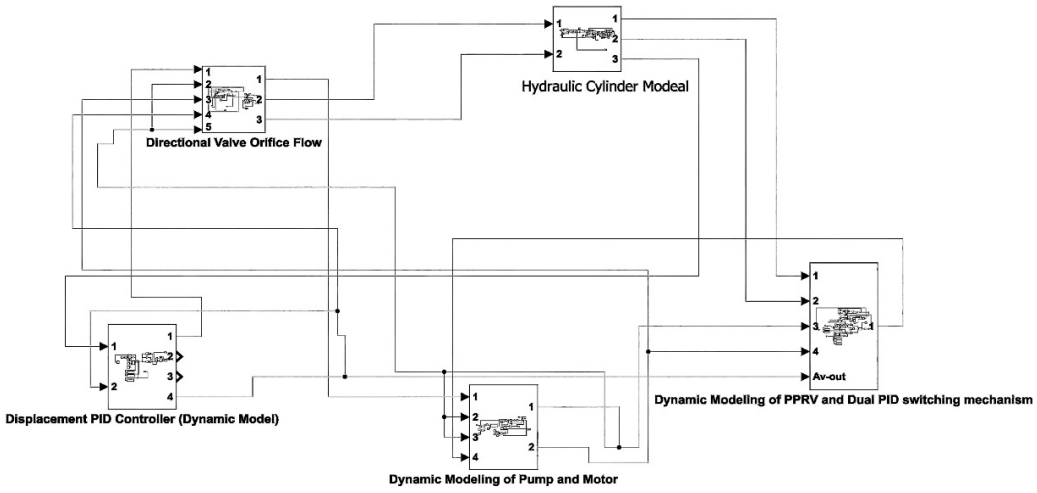

Fig. 7. Equation-based Simulink modeling of the electro-hydraulic elevator system.

B. Physical Modeling in Simulink Using Standard Simscape Blocks

Figure 8 depicts the entire simulated architecture of the electro-hydraulic elevator system. The model consists of a hydraulic cylinder, a proportional directional control valve that serves to control both flow and direction of hydraulic oil, a proportional pressure relief valve used to limit excessive pressure, a distance sensor that measures cabin height, and two pressure sensors at the cylinder ports. Each sensor is connected to a PID controller: one PID controls displacement via the directional valve, and two PID controllers regulate pressure via the proportional pressure relief valve. A switching logic selects the pressure controller to be used depending on the direction of motion. In this sense, port A is active during upward travel (e.g., first floor at 10 cm), whereas port B is activated during

downward travel (e.g., ground floor at 0 cm). The pressure controllers actuate a proportional pressure relief valve modeled as a variable-overlap orifice, proving accurate and dynamic pressure regulation. This model functions as the basis for comparing traditional PID control with optimization-based approaches such as PSO and CO.

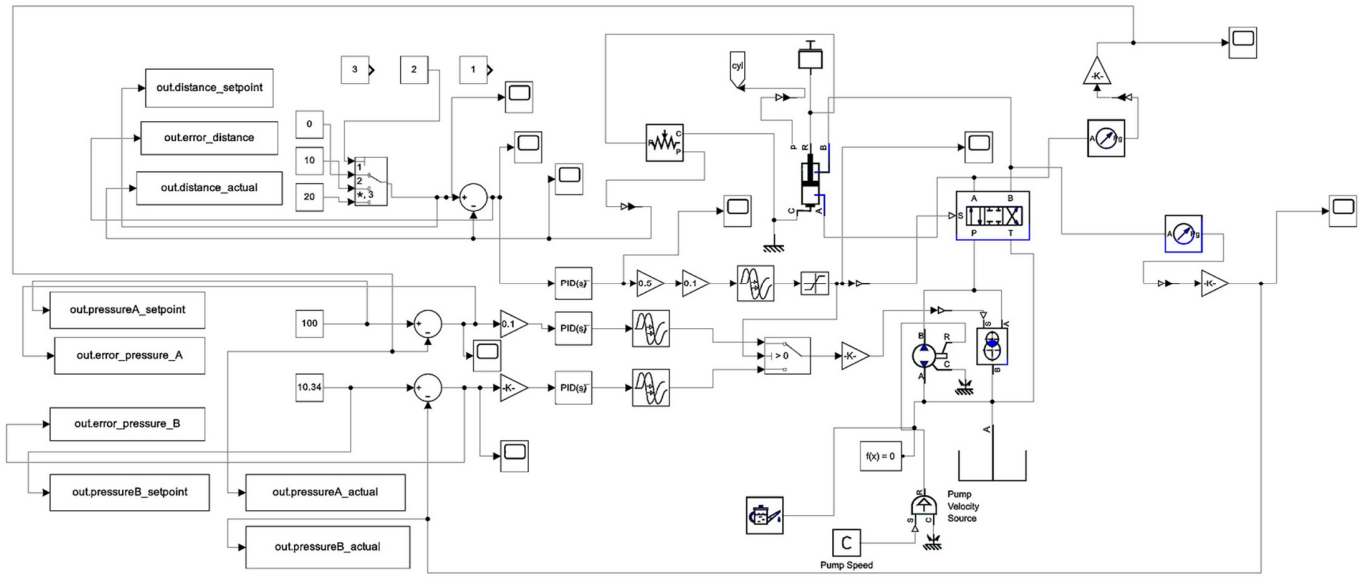

Fig. 8. Simulink-based physical model of the electro-hydraulic elevator developed using Simscape Fluids.

Table I lists the parameters employed in the Simscape-based physical model, reproducing the real operating conditions of the elevator. They include hydraulic oil properties, cylinder and pump dimensions, leakage coefficients, and initial conditions. The values were obtained either by estimation according to the design developed in this study or from component datasheets.

TABLE I. PARAMETERS ADOPTED IN THE HYDRAULIC ELEVATOR SIMULATION MODEL

Component	Description
Fixed-displacement pump	Pump displacement: 1.273×10^{-6} m^3·rad^{-1} Volumetric efficiency: 95% Total efficiency: 85% Nominal pressure: 10 MPa Angular velocity: ω_m = 157 rad·s^{-1} Fluid density: 880 kg·m^{-3}
Isothermal liquid predefined properties	Fluid: Hydraulic Oil ISO VG 46 Volumetric fraction of entrained air: 0.005 System temperature: 40 °C
4-way 3-position directional valve	Maximum opening: 0.005 m Critical Reynolds number: 150 Effective leakage area: 1×10^{-9} m^2
Proportional pressure relief valve	Variable overlapping orifice block employed to accurately simulate valve behavior; configured to closely match real valve characteristics due to the absence of a dedicated in Simulink
Double-acting actuator (IL)	Piston area A: 0.00196 m^2; Piston area B: 0.00102 m^2 Piston stroke:0.25 m; Dead volume: 1×10^{-5} m^3
Two pressure sensors (IL)	Each sensor is linked to its own PID block for precise pressure control at cylinder ports A and B
Ideal translational motion sensor	Initial position: 0 cm (ground floor)
Load	Cabin weight: 5 kg; Load weight: 30 kg

III. METHODOLOGY

A. Hydraulic System Modeling

The hydraulic system consists of several key components working together. It is one of the most important elements in the design of an electro-hydraulic elevator model and includes a double-acting hydraulic cylinder with a 25 cm stroke. To control the flow and direction of the system, a 4/3 proportional directional control valve for controlling the direction of hydraulic fluid flow (Rexroth, Model 4WREE 6 E08-24/G24K31/A1V, Reference No. R900912156, Serial No. 11, Batch No. 5411) is used. The valve spool type is directly operated and powered by a 24V DC solenoid. A proportional pressure relief valve is used for system safety and pressure regulation (Rexroth, Model DBEP 6 A06-13/45A624K4M, MNR: R90095507, SN:1, FD:4). It operates with a 24V DC solenoid and allows precise proportional adjustment of system pressure based on the reference input signal.

The system uses a fixed-displacement hydraulic pump powered by a three-phase electric motor connected to an AC power source located above the tank. The pump and tank are supplied by the Rexroth AG, Switzerland (RR Auftrag Nr: BW, Tank capacity: 30 kg, suitable for mineral oil HLP according to DIN 51525). The pump operates at a speed of 1,500 rpm, is matched to the system's requirements, and is designed for reliable operation with standard hydraulic oil. The tank contains an internal filter to purify the hydraulic fluid from impurities and protect system components.

The hydraulic cylinder, proportional directional valve, proportional pressure relief valve, and pump ensure smooth, efficient, and safe operation of the elevator under various load

conditions, as shown in Figures 9 and 10. The prototype components include: (1) a tank, (2) an electrical motor, (3) a constant-displacement pump, (4) a hydraulic cylinder, (5 & 6) pressure sensors, (7) a proportional directional control valve, (8) a gauge pressure, (9) a proportional pressure relief valve, (10) a distance sensor, (11) an elevator cabin, and (12) a control panel.

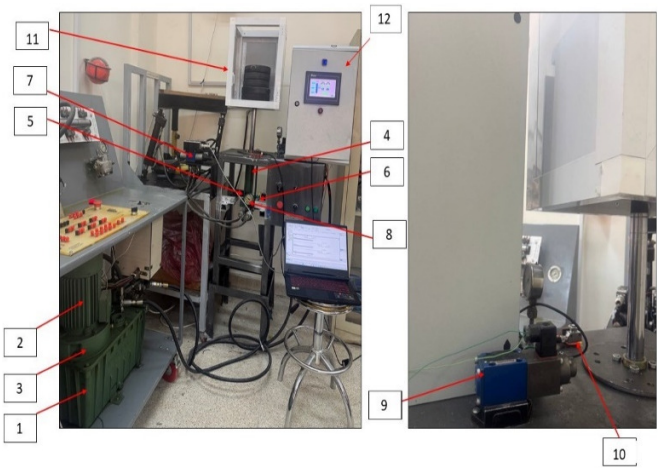

Fig. 9. Practical implementation of the electro-hydraulic elevator system.

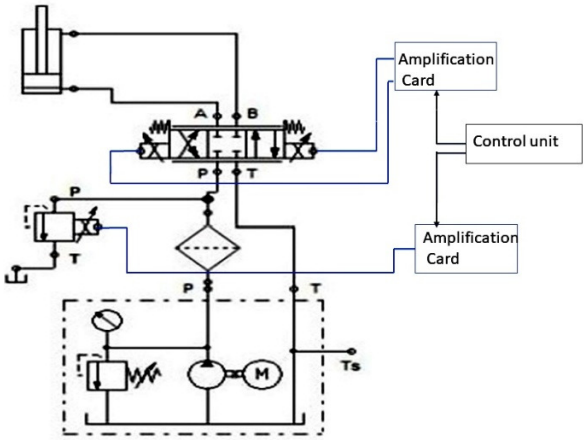

Fig. 10. Hydraulic circuit diagram of the electro-hydraulic elevator system.

B. Electrical Components

1) Ultrasonic Distance Sensor

The UGT585 distance sensor was applied to precisely measure the cabin height continuously over a range from 80 mm to 1,200 mm. The sensor provides an analog 0–10 V output and a digital (PNP) switching output, and is powered by a supply voltage of 10–30 V DC with a maximum current of 100 mA. It has an IP67 protection class, ensuring reliable operation in industrial environments. The analog output is hardwired to the PID module of the PLC, which in turn generates a signal proportional to the desired displacement, controlling the cabin speed through a proportional directional control valve. Unlike standard limit switches that only provide discrete on/off signals, this sensor provides dust-proof and vibration-tolerant measurements. This enables higher accuracy of position during movement and easy interfacing with the PID module in the PLC for real-time closed-loop control; that is, smoothness and reliability of cabin movement are enhanced, particularly under changing load circumstances or operation perturbations. Thus, this ultrasonic sensor improves position-tracking performance and offers better reliability and accuracy for the elevator system compared with conventional sensors.

2) Pressure Sensors

Two pressure sensors (0–10 V analog output) are used to regulate hydraulic pressure through the proportional pressure relief valve. Each sensor is connected to the PID module inside the PLC. Sensor A monitors pressure during upward cabin movement, and sensor B during downward movement. The proportional pressure relief valve is integrated within a closed-loop control system incorporating a PID controller and these two pressure sensors. This configuration minimizes pressure fluctuations and provides high stability under changing loads. The simple safety valve has been converted to a dynamically controlled pressure valve within the circuit. The electrical control panel consists of the PLC, input/output units, relays, and an amplifier card that drives the proportional pressure relief valve. The desired floor is selected through the HMI interface, as illustrated in Figure 11.

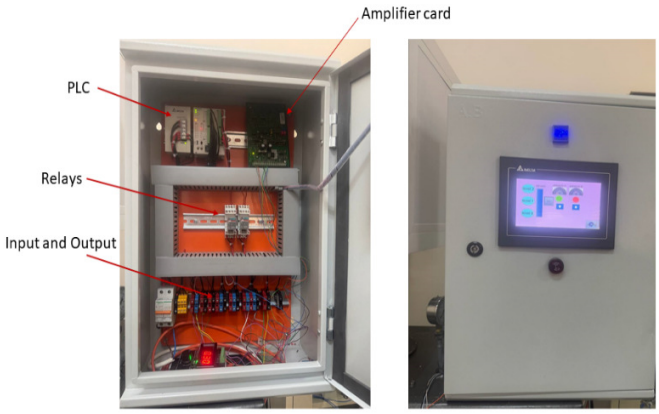

(a) (b)

Fig. 11. Control system overview: (a) electrical control panel of the system, (d) Delta HMI screen.

C. Controller

1) PLC Controller

A PLC is a centralized control unit that is widely used in industrial applications. In this project, a DVP-20SX2 was employed to implement control, process sensor signals, and issue commands to the proportional valves. The sensors provide feedback to the PID controllers integrated within the PLC. The measured signals are compared to reference values corresponding to predefined floors or pressure set points. The PID output is then sent through analog channels (±10V) to control the proportional directional valve and the proportional pressure relief valve. Ladder Logic control was implemented using the ISPSoft software. The PLC also provides seamless

integration with the HMI, simplifying floor selection for the user.

2) PID Controller

A PID controller is a feedback-based loop control mechanism used to regulate variables such as pressure and speed. The algorithm compares the measured value against the desired reference, determines the error, and dynamically adjusts control inputs in real time. The proportional component (P) corrects deviations immediately in proportion to the error magnitude. The integrative component (I) accumulates past errors to eliminate steady-state offset. The derivative component (D) predicts the future rate of change of the error to enhance stability and responsiveness. Mathematically, the PID module is represented as follows [25]:

$$u(t) = K_P\, e(t) + K_I \int_0^t e(t)dt + K_D \frac{de(t)}{dt} \quad (15)$$

where K_P is the proportional gain, K_I is the integral gain, K_D is the derivative gain, and $e(t)$ denotes the difference between the set point and the measured value.

3) Particle Swarm Optimization Algorithm

PSO is a population-based algorithm inspired by the collective motion of birds or fish. Its application can be seen in a wide variety of areas, from machine learning to engineering design. It uses a population of possible solutions to reach an optimum solution within the search space. Each particle updates its position based on its own best experience and the best experience of the entire swarm [26].

4) Cheetah Optimizer Algorithm

The CO is a modern algorithm inspired by cheetah hunting behavior and is characterized by simple calculations and rapid convergence to optimal solutions with minimal parameter tuning [27]. It consists of three phases:

- Exploration phase: The cheetah seeks an opportunity to hunt by observing prey. The cheetah moves or remains stationary depending on its physical condition and the availability of prey. This phase is represented as follows:

$$X_{\{i,j\}}^{\{t+1\}} = X_{\{i,j\}}^{t} + r_{\{i,j\}}^{\{-1\}}\, \alpha_{\{i,j\}}^{t} \quad (16)$$

  where $X_{\{i,j\}}^{t}$ and $X_{\{i,j\}}^{\{t+1\}}$ represent the current and updated positions for cheetah i in dimension j; t represents the current hunting time; T is the maximum hunting duration; $r_{\{i,j\}}^{\{-1\}}$ denotes the randomization parameter generated from the standard normal distribution; and $\alpha_{\{i,j\}}^{t}$ is the step length, which is often defined as $0.001\times t/T$.

- Sit-and-wait phase: The cheetah adopts an ambush strategy to avoid alerting the prey. Instead of moving actively, the cheetah hides or remains in position and waits for the prey to approach. This is mathematically represented as follows:

$$X_{\{i,j\}}^{\{t+1\}} = X_{\{i,j\}}^{t} \quad (17)$$

  Here, $X_{\{i,j\}}^{t}$ and $X_{\{i,j\}}^{\{t+1\}}$ represent the current and updated positions for cheetah i in dimension j, respectively.

- Attack phase: The cheetah rapidly updates the operator's position, both individually and collectively, based on the best-known locations according to optimum solutions. These dynamic adjustments enhance the ability of the algorithm in the rapid convergence toward optimum results. This is mathematically represented as follows:

$$X_{\{i,j\}}^{\{t+1\}} = X_{\{B,j\}}^{t} + r_{\{i,j\}}\beta_{\{i,j\}}^{t} \quad (18)$$

  where $X_{\{B,j\}}^{t}$ represents the current best (prey) position in the j-th dimension; $\beta_{\{i,j\}}^{t}$ denotes the interaction factor between cheetah i and either a neighboring cheetah or the leader; and the term $r_{\{i,j\}}$ is a random variable drawn from a standard normal distribution.

5) PID Optimization Setup and Objective Function

This section describes the use of baseline values for each method within the standard range and the verification of their stability to ensure a fair comparison between optimization algorithms. The number of iterations was determined based on convergence analysis to balance computational efficiency and system stability, as shown in Table II.

TABLE II. TUNING PARAMETERS FOR THE PSO AND CO OPTIMIZATION TECHNIQUES

Parameter	PSO	CO
Population size	30	20
Iterations	50	40
W	0.7	—
C_1	1.5	—
C_2	1.5	—
α	—	2.5
β	—	0.3
K_P bounds	0	100
K_I bounds	0	50
K_D bounds	0	20

The PID parameters were chosen to be broad enough to encompass all optimal solutions obtained during the optimization process, while simultaneously avoiding unnecessarily expanding the search space. The optimization process is terminated either when the maximum number of iterations is reached (50 for the PSO algorithm and 40 for the CO algorithm) or when the optimization in the Integral Time-weighted Absolute Error (ITAE) is not excessive. This ensures both computational efficiency and system stability.

The objective function used is the ITAE, represented as follows:

$$J = \int_0^T t \cdot |e(t)|dt \quad (19)$$

Here, $e(t)$ represents the difference between the desired value and the actual value at a given time, and T is the time over which the system is evaluated.

For multiple control loops, the total objective is calculated as a weighted sum:

$$J_{total} = w_d \cdot J_{distance} + w_p \cdot J_{pressure} \quad (20)$$

where J_{total} denotes the overall value of the objective function; $J_{distance}$ represents the ITAE for the distance control loop; and $J_{pressure}$ is the ITAE for the pressure control loop.

All regulatory constraints, such as actuator limits and allowable ripple, were applied. Furthermore, the same objective function was used for both the PSO and CO algorithms, ensuring a fair comparison and applicability to the electro-hydraulic elevator.

6) PLC Implementation

The PID controllers were implemented in the PLC using Ladder Logic with integrated PID modules. A direct mapping from simulation to real-world hardware was followed. Initially, the PID controller parameters were configured using MATLAB/Simulink to determine the optimal parameters for each method and record the system response. Then, the parameters for each PID control method (conventional, PSO-PID, and CO-PID) were manually entered into the PLC's PID modules. The values of P, I, and D were multiplied by 100 before input to match the internal scale of the PID modules, which internally divides the input by 100.

All sensors provided analog outputs (0–10 V) representing their measurement range. These signals were converted to the corresponding physical values: displacement in mm for the distance sensor and pressure in Pa for the pressure sensors, before being fed into the PID modules to ensure accuracy between the actual system variables and the controller inputs.

Additionally, the sampling time was implemented in the PID module as a variable parameter adjustable via the HMI, allowing real-time response adjustment and flexible control. No filter was applied in this implementation because the sensors provide sufficiently high accuracy, the nature of the elevator's movement does not require additional filtering, and the digital operations and derivative computations are handled internally by the PLC.

IV. RESULTS AND DISCUSSION

Both a traditional PID controller and optimization-based PID controllers were employed to evaluate the performance of the hydraulic elevator system. The results are organized into two main parts. The first part presents the simulation results obtained in the MATLAB/Simulink environment, where a conventional PID controller was initially used as a baseline and then enhanced using the PSO and CO algorithms. The second part reports the practical implementation results obtained from experimental tests conducted on a physical hydraulic elevator prototype.

The PID controller implemented in the Delta PLC utilized the optimized controller parameters derived from the simulation study. Three different sets of PID parameters were examined: the original manually tuned PID parameters, the PSO-optimized parameters, and the CO-optimized parameters. Although the experimental response included both upward and downward motions of the elevator cabin, only the ascending responses were considered for comparison with the simulation results. This selection is justified because the upward displacement motion has the greatest influence on the system's dynamic behavior and is therefore the most representative case for evaluating controller performance and validating the simulation model.

To maintain consistency between the simulation and experimental environments, the same time scale was used on the horizontal axis in both cases. In the simulation, the elevator reaches the reference levels of 10 cm and 20 cm at 10 s; therefore, the experimental measurements corresponding to these levels were taken at the same time instants. This synchronization ensured a fair and accurate comparison among the three methods and reduced discrepancies arising from time misalignment.

A. Simulation Results

In this simulation study, the performance of an electro-hydraulic elevator system under three different control strategies (conventional PID, PSO-PID, and CO-PID) was investigated in the MATLAB/Simulink environment. The mathematical model was validated, and the efficiency of the optimization algorithms was assessed for two displacement values of 10 cm and 20 cm under maximum load conditions. For each case, the calculated performance indicators are: ascent time, settling time, overshoot ratio, steady-state error, and ITAE.

1) Simulation Results using the Conventional PID Controller

The essential performance of the system was first tested using a conventional PID controller, whose parameters are presented in Table III. Figure 12 illustrates the displacement responses of the 10 cm and 20 cm set points. This controller successfully drove the system to the reference values within 5–6 s with relatively smooth movement and small steady-state error. Pressure responses at ports A and B showed a brief initial delay because of the switching logic, and then converged to the reference values with acceptable accuracy.

In general, the conventional PID showed fair tracking performance; however, the stabilization time was moderate, and the pressure steady-state error was slightly higher compared with displacement. As shown in Table IV, the conventional PID controller yields an ITAE of 5,606.36, which is used as a baseline for comparison with the PSO and CO optimizations.

TABLE III. PARAMETERS OF THE CONVENTIONAL PID CONTROLLER

Controller type	K_P	K_I	K_D
Distance PID controller	15.0000	0.0300	8.0000
Pressure A PID controller	15.0000	1.0000	0.8000
Pressure B PID controller	12.0000	0.7000	0.6000

TABLE IV. SIMULATION RESULTS IN MATLAB USING THE CONVENTIONAL PID CONTROLLER

Parameter	Rise time (s)	Settling time (s)	Steady-state error
Distance at 10 cm set point	4.551	5.430	0.0536
Distance at 20 cm set point	4.000	6.050	0.0435
Pressure B (10.34 bar)	6.700	7.100	0.0501
Pressure A (100 bar)	7.000	7.100	0.0400

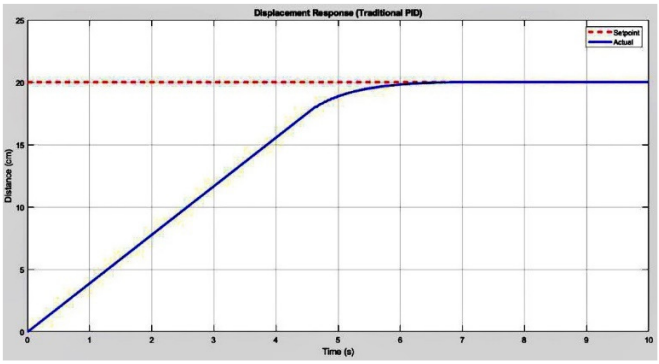

(a)

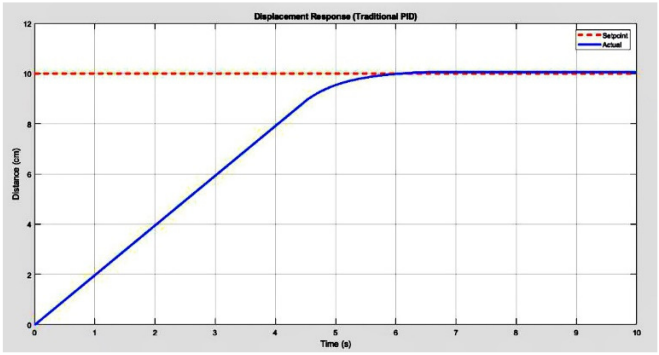

(b)

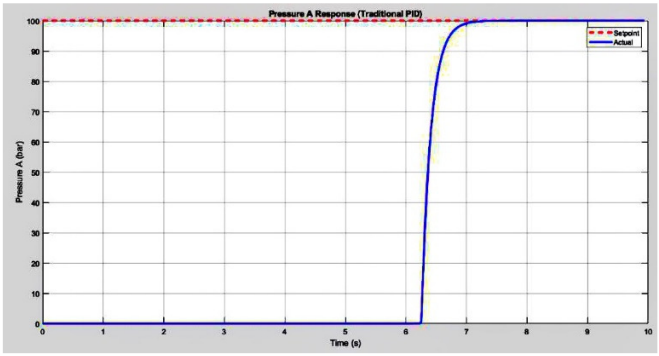

(c)

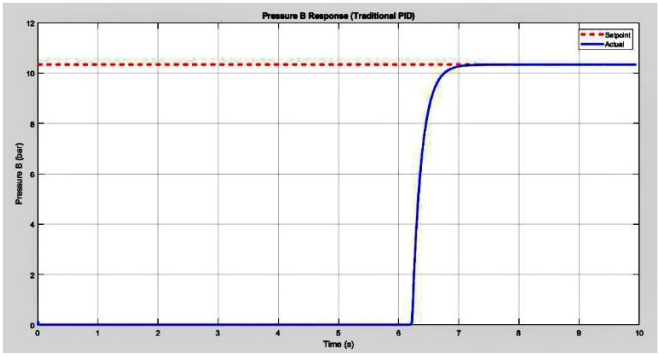

(d)

Fig. 12. Displacement and pressure responses for the hydraulic elevator system using conventional PID control: (a) displacement response at the 20 cm reference level, (b) displacement response at the 10 cm reference level, (c) pressure response at port A for a 100 bar set point, (d) pressure response at port B for a 10.34 bar set point.

2) Simulation Results Using the PSO-PID Controller

To enhance the hydraulic elevator system's dynamic response and ensure precise displacement and pressure regulation, the PSO algorithm was used to fine-tune the PID controller parameters. The PID parameters optimized by the PSO algorithm are shown in Table V.

TABLE V. PARAMETERS OF THE PSO-PID CONTROLLER

Controller type	K_P	K_I	K_D
Distance PID controller	42.5889	0.0382	2.3782
Pressure A PID controller	13.0342	0.0143	0.5921
Pressure B PID controller	31.8804	0.0183	0.3599

The simulation results obtained with the PSO-PID controller are shown in Figure 13. Both displacement and pressure responses demonstrate a clear improvement in system performance. In particular, the rise and settling times were significantly shorter than those of the traditional PID controller. Additionally, the system showed little overshoot and an almost insignificant steady-state error as it quickly reached reference values, as shown in Table VI. Compared to the baseline ITAE of 5,606.36 obtained with the traditional PID controller, the PSO-PID controller achieved a lower ITAE of 5,555.8793.

TABLE VI. SIMULATION RESULTS IN MATLAB USING THE PSO-PID CONTROLLER

Parameter	Rise time (s)	Settling time (s)	Steady-state error
Distance at 10 cm set point	4.551	4.954	0.0220
Distance at 20 cm set point	3.106	3.969	0.0200
Pressure B (10.34 bar)	6.000	6.100	0.0400
Pressure A (100 bar)	5.800	6.000	0.0330

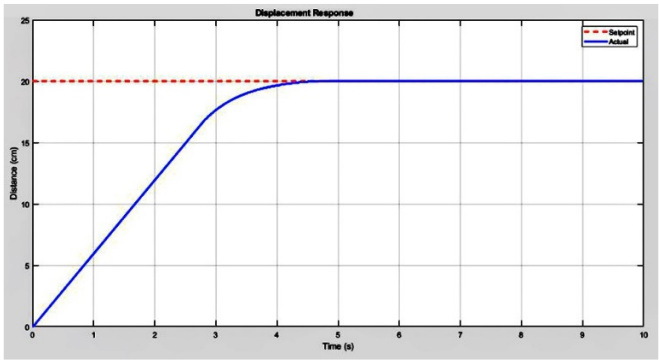

(a)

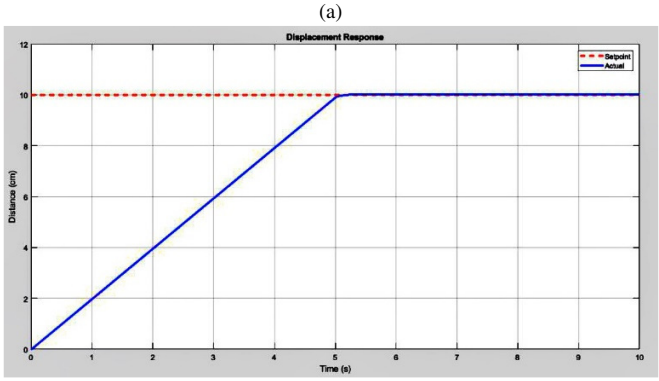

(b)

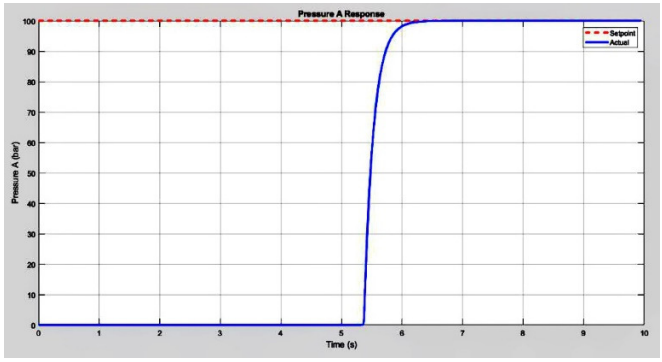

(c)

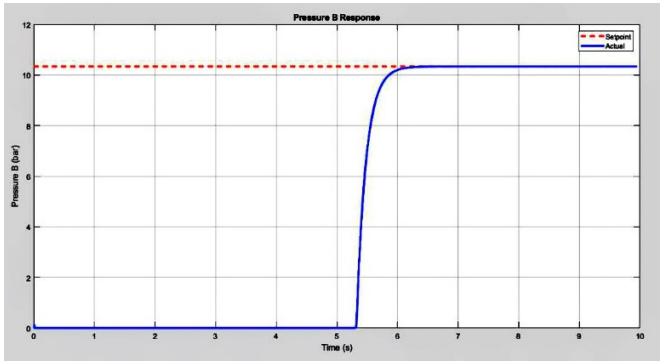

(d)

Fig. 13. Displacement and pressure responses for the hydraulic elevator system using PSO-PID control: (a) displacement response at the 20 cm reference level, (b) displacement response at the 10 cm reference level, (c) pressure response at port A for a 100 bar set point, (d) pressure response at port B for a 10.34 bar set point.

3) Simulation Results Using the CO-PID Controller

The simulation results obtained with the CO-PID controller are presented in this section. The PID parameters optimized by the CO algorithm are shown in Table VII.

TABLE VII. PARAMETERS OF THE CO-PID CONTROLLER

Controller type	K_P	K_I	K_D
Distance PID controller	26.4637	0.0190	1.7532
Pressure A PID controller	29.6938	0.0302	0.9510
Pressure B PID controller	30.1555	0.0432	0.6153

The CO-PID controller significantly reduced the rise and settling times compared with both the PSO-PID and conventional PID controllers. The steady-state error at the 20 cm set point decreased from 0.0200 (using PSO-PID) to 0.0100 with CO-PID, whereas the total ITAE decreased from 5,555.8793 to 5,539.4287. In addition, the system's dynamic response and control accuracy were further enhanced. These findings demonstrate that the CO algorithm can finely adjust the PID parameters to achieve improved system performance.

The hydraulic elevator system's dynamic performance metrics using the CO-PID controller are summarized in Table VIII and illustrated in Figure 14. Although the switching logic applied to the pressure signals introduces a slight initial delay before PID activation, the response becomes noticeably more accurate and stable after activation. The numerical improvement in ITAE between PSO-PID and CO-PID is relatively small, which is expected since the PSO algorithm already converges close to the optimal solution. Consequently, the CO algorithm performs refined fine-tuning, producing a clearly observable improvement in response speed and overall dynamic performance. Overall, these findings confirm that the CO-PID controller can achieve superior control accuracy and stability, making it highly suitable for the hydraulic elevator system.

TABLE VIII. SIMULATION RESULTS IN MATLAB USING THE CO-PID CONTROLLER

Parameter	Rise time (s)	Settling time (s)	Steady-state error
Distance at 10 cm set point	3.642	3.965	0.0221
Distance at 20 cm set point	3.012	3.279	0.0100
Pressure B (10.34 bar)	5.700	5.900	0.0300
Pressure A (100 bar)	5.600	5.900	0.0300

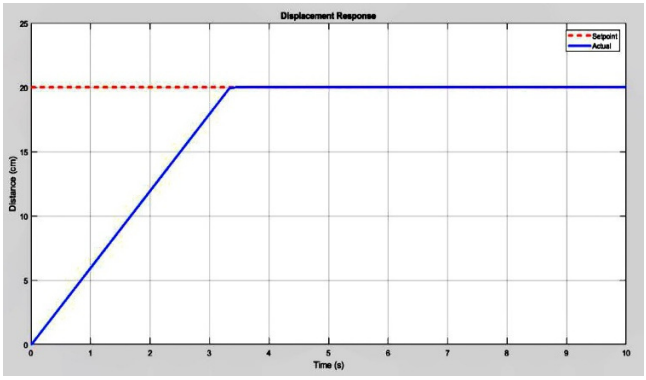

(a)

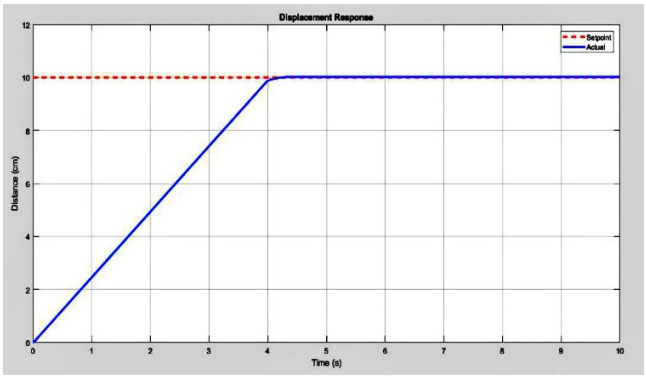

(b)

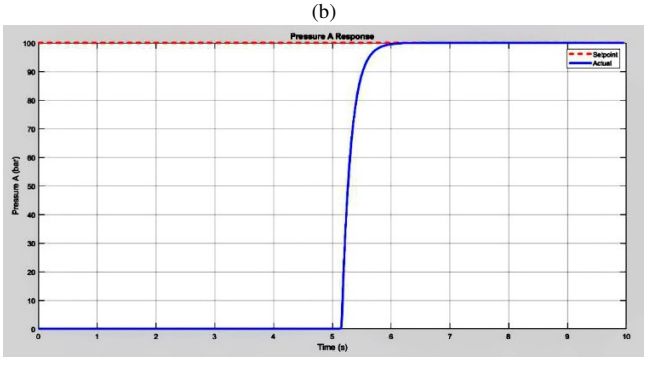

(c)

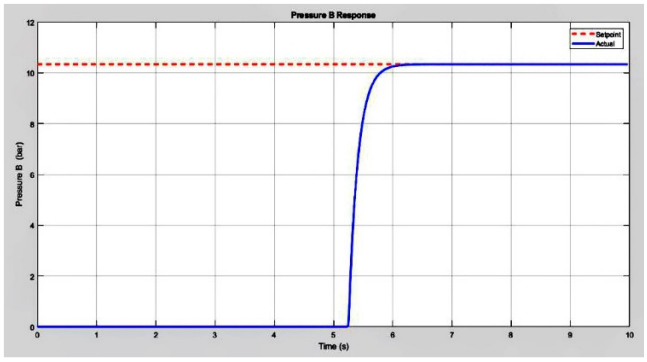

(d)

Fig. 14. Displacement and pressure responses for the hydraulic elevator system using CO-PID control: (a) displacement response at the 20 cm reference level, (b) displacement response at the 10 cm reference level, (c) pressure response at port A for a 100 bar set point, (d) pressure response at port B for a 10.34 bar set point.

B. Practical Implementation Results

In this practical section, the electro-hydraulic elevator was experimentally tested to validate the simulation results and assess its performance under real operating conditions. Simulations were performed at the maximum load (30 kg) as the most demanding case for controller tuning. Experiments included both no-load tests, to examine system stability, and loaded tests (10–30 kg) to evaluate control effectiveness. When there was no load, the answers were faster because of lower weight. However, the order of performance of the controllers remained the same: CO-PID outperformed PSO-PID, which in turn outperformed the conventional PID. An initial response delay of approximately 5 s for displacement and 5.2 s for pressure was observed. This delay is considered normal and results from inherent system characteristics such as valve response, friction, oil compression, and chamber filling.

In the no-load condition, conventional PID, PSO-PID, and CO-PID controllers were examined to assess the system's stability and response, as depicted in Figure 15. Calculations were performed during the 0–10 s window from the step input. The conventional PID at a 10 cm set point demonstrated a rise time of ~5.0 s, a settling time of ~6.6 s, and a steady-state error of ~0.18 cm. The improvement brought about by the PSO-PID included rise times of 3.15 s, a settling time of 4.15 s, and a steady-state error of 0.03 cm. The best performance was attained by the CO-PID controller, which exhibited a rise time of ~2.75 s, settling time of ~3.6 s, and steady-state error ≤ 0.03 cm. At the 20 cm set point, the conventional PID showed a rise time of ~3.5 s, a settling time of ~5.0 s, and a steady-state error of ~0.18 cm. The PSO-PID reduced these values to ~2.2 s, ~3.15 s, and ~0.03 cm, respectively, whereas the CO-PID provided the fastest and most accurate response with a rise time of ~1.9 s, settling time of ~2.75 s, and steady-state error ~0.03 cm.

In the pressure responses (Figures 16 and 17), the CO controller achieved the fastest performance. At port A, the rise time was ~5.78 s with a final error of ~0.0169 bar, and at port B, the rise time was ~5.85 s with a final error of ~0.0032 bar. Settling times did not exceed 5.9–6.0 s. The PSO controller was slightly slower, with rise times of ~5.88 s (port A) and ~5.91 s (port B), final errors of ~0.0223 bar and ~0.0058 bar, and settling times of 6.03–6.08 s. The conventional PID showed the slowest response, with rise times of ~6.18 s (port A) and ~6.20 s (port B), final errors of ~0.0108 bar and ~0.0127 bar and settling times of 6.42–6.45 s.

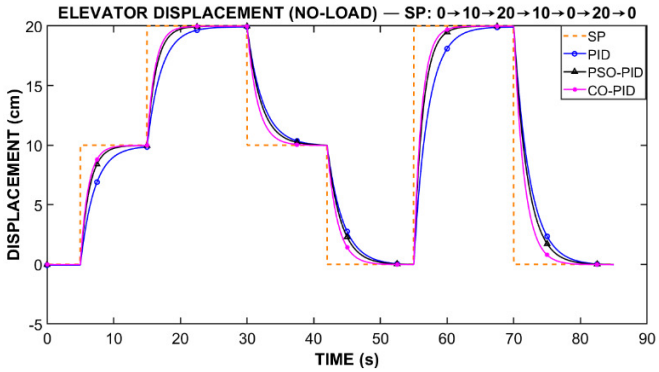

Fig. 15. Cabin displacement response under the no-load condition using three control strategies (PID, PSO-PID, and CO-PID).

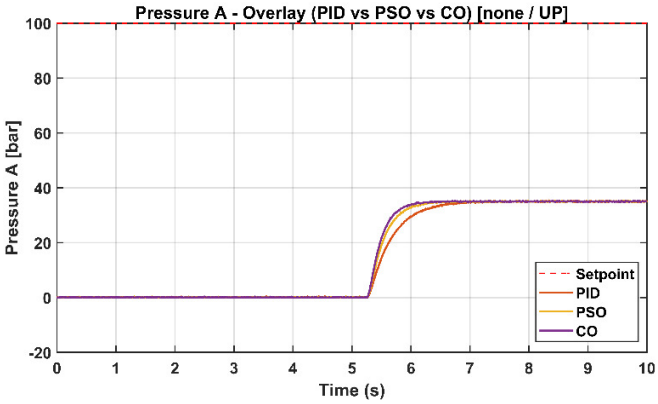

Fig. 16. Pressure response at port A (no-load) for PID, PSO-PID, and CO-PID.

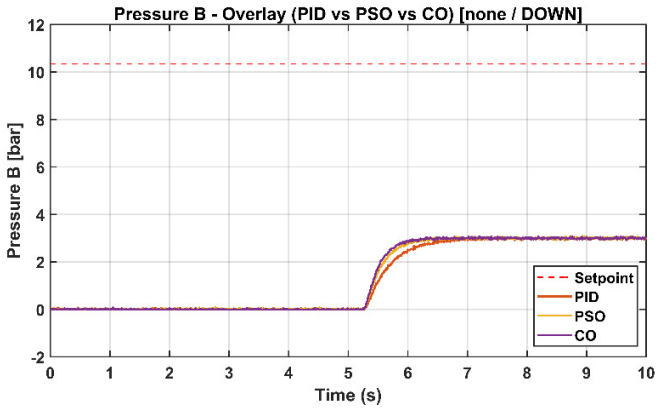

Fig. 17. Pressure response at port B (no-load) for PID, PSO-PID, and CO-PID.

After evaluating the no-load performance, the elevator was tested under a 10 kg load to assess its effect on response and

control accuracy. Displacement responses for the three controllers (PID, PSO-PID, CO-PID) are shown in Figure 18. For the conventional PID, the response slowed with load: at the 10 cm step, rise time was 5.5 s, settling time 7.3 s, and steady-state error 0.237 cm; at 20 cm, rise time was 3.85 s, settling time 5.55 s, and steady-state error 0.239 cm. PSO-PID improved performance, with rise times of 3.5 s and 2.45 s, settling times of 4.55 s and 3.5 s, and steady-state errors of 0.0449 cm and 0.045 cm. CO-PID performed best, achieving rise times of 3.0 s and 2.1 s, settling times of 3.95 s and 3.0 s, and steady-state errors of 0.0322 cm and 0.032 cm. Under a load of 10 kg, the CO-PID controller achieved the most accurate and stable response, surpassing PSO-PID and traditional PID.

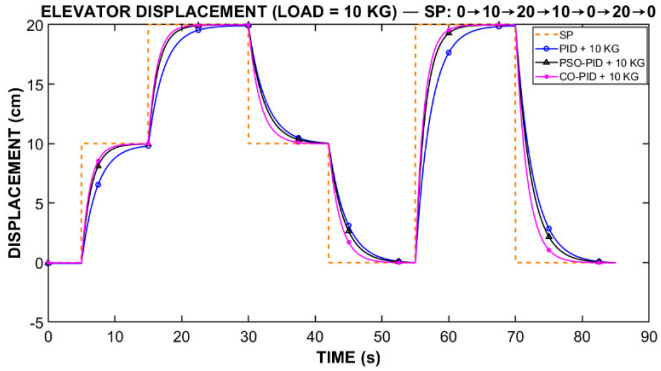

Fig. 18. Cabin displacement response under a 10 kg load using three control strategies (PID, PSO-PID, and CO-PID).

Figures 19 and 20 present the pressure responses for port A and port B, respectively, under a 10 kg load. The CO-PID controller achieved the best performance: for port A, a rise time of 5.89 s, a settling time of 6.20 s, and a steady-state error of 0.0117 bar; and for port B, a rise time of 5.95 s, a settling time of 6.34 s, and a steady-state error of 0.0149 bar. The PSO-PID controller was slightly slower: port A had a rise time of 6.02 s, a settling time of 6.39 s, and a steady-state error of 0.0370 bar; port B showed a rise time of 6.05 s, a settling time of 6.48 s, and a steady-state error of 0.0119 bar, still outperforming the conventional PID in accuracy. The conventional PID was the slowest, with port A having a rise time of 6.37 s, a settling time of 7.0 s, and a steady-state error of 0.0181 bar; port B having a rise time of 6.43 s, a settling time of 7.14 s, and a steady-state error of 0.0233 bar, showing reduced accuracy under load. Adding a 10 kg load slightly increased rise and settling times (~0.2–0.5 s); the CO-PID remained the fastest, followed by PSO-PID, then the traditional PID.

For a 15 kg load, the displacement responses of the electro-hydraulic elevator system exhibited clear differences among the controllers (Figure 21). For the first reference step (0–10 cm), the conventional PID showed the slowest response, with a rise time of 5.8 s, settling time of 7.65 s, and steady-state error of 0.28 cm. The PSO-PID improved performance, achieving a rise time of 3.65 s, settling time of 4.8 s, and steady-state error of 0.06 cm. The CO-PID outperformed both, with a rise time of 3.15 s, settling time of 4.15 s, and a minimal steady-state error of 0.02 cm. For the second step (0–20 cm), the trend was similar: the conventional PID exhibited a rise time of 4.05 s, settling time of 5.8 s, and steady-state error of 0.27 cm; PSO-PID showed a rise time of 2.55 s, settling time of 3.65 s, and steady-state error of 0.05 cm; CO-PID achieved the fastest rise time of 2.2 s, settling time of 3.15 s, and steady-state error of 0.04 cm. With increased load, PSO-PID and CO-PID controllers outperformed the traditional PID controller, with CO-PID achieving more accurate and stable performance.

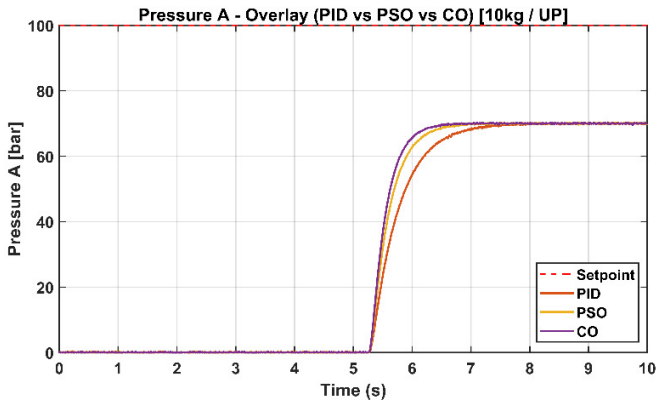

Fig. 19. Pressure response at port A under 10 kg load for PID, PSO-PID, and CO-PID.

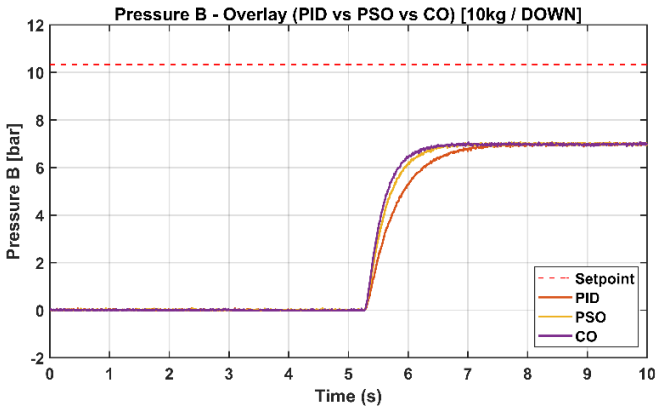

Fig. 20. Pressure response at port B under 10 kg for PID, PSO-PID, and CO-PID.

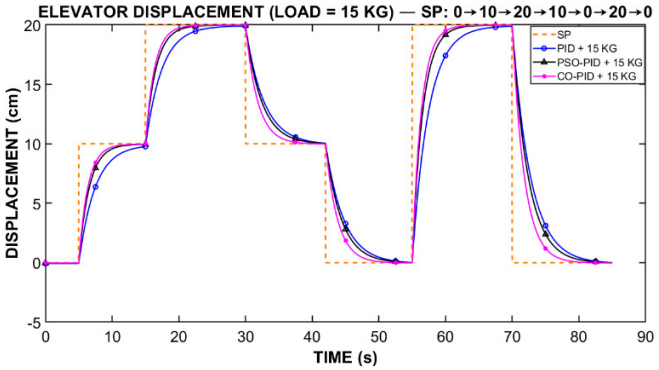

Fig. 21. Cabin displacement response under a 15 kg load using three control strategies (PID, PSO-PID, and CO-PID).

The pressure responses of the elevator for ports A and B, under a load of 15 kg (Figures 22 and 23) were also evaluated. Using the CO-PID controller, settling times of 6.43 s (port A) and 6.54 s (port B) were achieved, with low steady-state errors of 0.0051 bar and 0.0028 bar, respectively. The PSO-PID controller was slightly slower, with settling times of 6.66 s (port A) and 6.79 s (port B), and steady-state errors of 0.0210 bar and 0.0071 bar, respectively. The conventional PID showed the slowest response, with settling times of 7.3 s (port A) and 7.63 s (port B), and steady-state errors of 0.0148 bar and 0.0144 bar. These results indicate that increasing the load moderately increased settling times (~0.3–0.6 s) and steady-state deviations due to higher hydraulic resistance and system inertia. Nevertheless, the controller ranking remained consistent: CO-PID delivered the highest accuracy and dynamic stability, followed by PSO-PID, and then conventional PID with the largest deviations.

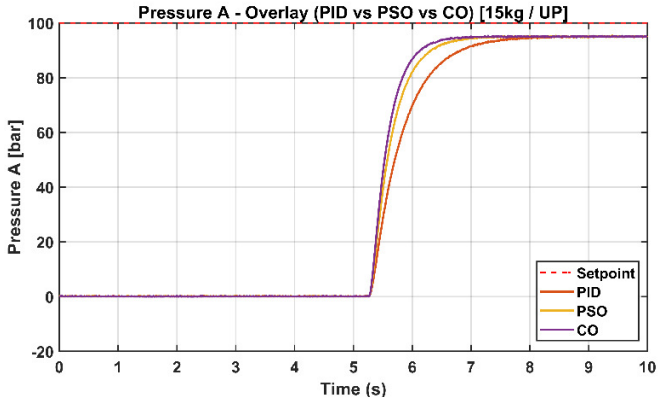

Fig. 22. Pressure response at port A under 15 kg load for PID, PSO, and CO-PID.

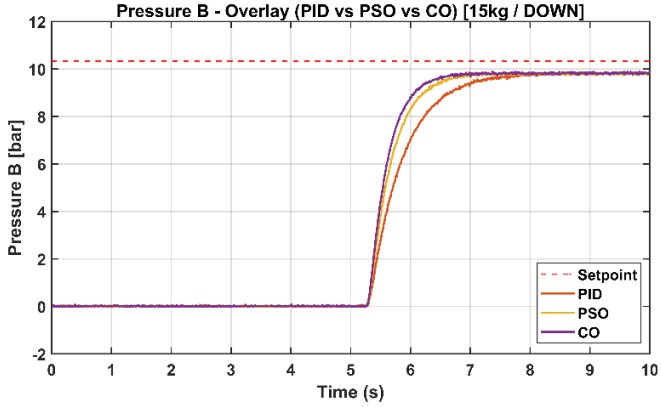

Fig. 23. Pressure response at port B under 15 kg load for PID, PSO-PID, and CO-PID.

The electro-hydraulic elevator was tested under a 30 kg load using PID, PSO-PID, and CO-PID controllers (Figure 24). For the first step (0–10 cm), PID showed the slowest response, with a rise time of 6.55 s, settling time of 8.7 s, and final error of 0.39 cm. PSO-PID improved performance to a rise time of 4.15 s, settling time of 5.45 s, and final error of 0.08 cm. CO-PID outperformed both, achieving a rise time of 3.6 s, settling time of 4.7 s, and final error of 0.05 cm. For the second step (0–20 cm), PID recorded a rise time of 4.6 s, settling time of 6.6 s, and final error of 0.4 cm; PSO-PID achieved 2.9 s, 4.15 s, and 0.08 cm; CO-PID again performed best with 2.5 s, 3.6 s, and 0.05 cm, respectively.

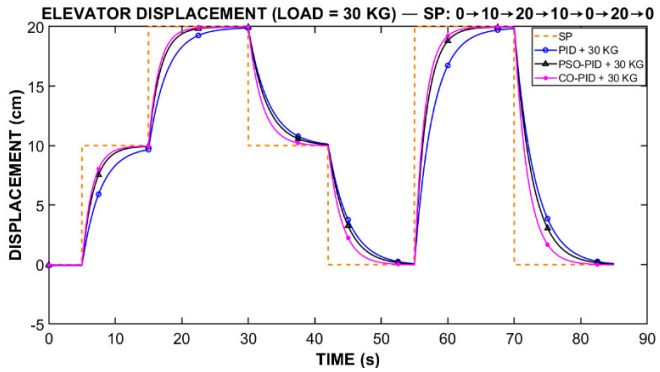

Fig. 24. Cabin displacement response under a 30 kg load using three control strategies (PID, PSO-PID, and CO-PID).

The experimental pressure responses of the three controllers under a maximum 30 kg load showed distinct differences. At port A, it can be observed from Figure 25 that CO-PID had the fastest settling time of 6.41 s with a final error of 0.033 bar, followed by PSO-PID at 6.67 s and 0.035 bar, whereas conventional PID was the slowest at 7.6 s and 0.04 bar. At port B, Figure 26 shows that CO-PID reaches its steady state in 6.62 s with a final error of 0.0065 bar, PSO-PID in 6.93 s with 0.0212 bar, and PID in 7.99 s with 0.03 bar. These results verify that intelligent optimization-based controllers outperform the conventional PID in terms of both stabilization speed and steady-state accuracy under maximum load.

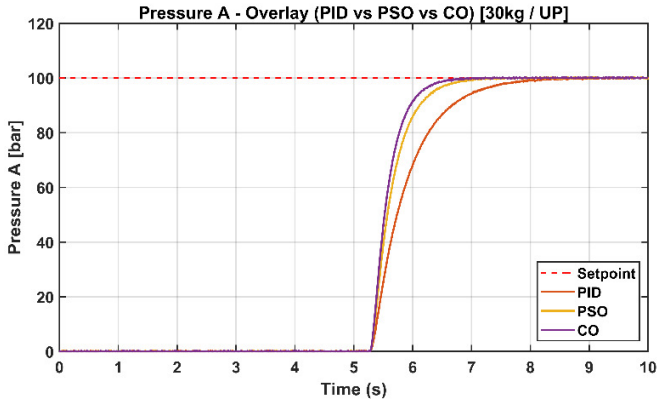

Fig. 25. Pressure response at port A under 30 kg load for PID, PSO-PID, and CO-PID.

C. Comparative Analysis between Experimental and Simulation Results at Maximum Load (30 kg)

A comprehensive comparative analysis was performed between the experimental results and MATLAB simulation outcomes of the electro-hydraulic elevator system under a maximum load of 30 kg. It was performed in an effort to investigate the accuracy of the simulation model in

representing the real system behavior with respect to displacement and pressure responses under three control strategies: conventional PID, PSO-PID, and CO-PID.

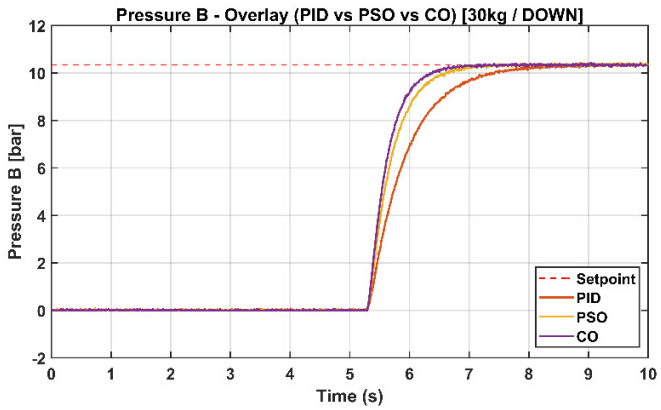

Fig. 26. Pressure response at port B under 30 kg load for PID, PSO-PID, and CO-PID.

All of these controllers presented the same ranking when it came to performance in both experiments and simulations, with CO-PID performing best, followed by PSO-PID, whereas conventional PID was the slowest and least precise. Slightly longer rise and settling times were observed in the experimental tests compared with the simulation results due to practical factors such as valve dynamics, sensor filtering, mechanical inertia, and friction. Throughout the displacement responses at a set point of 10 cm, the experimental rise and settling times for conventional PID were 6.55 s and 8.7 s, respectively, with a final error of 0.39 cm. In comparison, the corresponding simulation values were 4.55 s and 5.43 s, with a final error of 0.0536 cm. The PSO-PID controller achieved experimental rise and settling times of 4.15 s and 5.45 s, respectively, with a final error of 0.08 cm, whereas the simulation results yielded 4.55 s and 4.95 s, with a final error of 0.022 cm. The CO-PID controller outperformed both methods, achieving experimental rise and settling times of 3.6 s and 4.7 s, respectively, with a final error of 0.05cm. In simulation, the rise time slightly increased to 3.64 s, whereas the settling time decreased to 3.97 s, with a final error of 0.0221 cm. At a set point of 20 cm, the experimental rise and settling times were 4.6 s and 6.6 s for PID, 2.9 s and 4.15 s for PSO-PID, 2.5 s and 3.6 s for CO-PID, with corresponding final errors of 0.4 cm, 0.08 cm, and 0.05 cm, respectively.

Based on experimental results, CO-PID achieved reductions of 45.4% in rise time, 45.7% in settling time, and 87% in final error compared with the conventional PID controller. Relative to PSO-PID, the improvements were 13.6% in rise time, 13.8% in settling time, and 37.5% in final error. These results confirm that the CO-PID controller provides a precise and stable displacement response, resulting in smoother cabin movement, reduced overshoot, and improved positioning accuracy.

For pressure responses at port A, the experimental settling times were 7.6 s for PID, 6.67 s for PSO-PID, and 6.41 s for CO-PID, with final errors of 0.04 bar, 0.035 bar, and 0.033 bar, respectively. The corresponding simulation settling times were 7.1 s, 6.1 s, and 5.6 s, with final errors of 0.04 bar, 0.033 bar, and 0.03 bar. At port B, the experimental settling times were 7.99 s, 6.93 s, and 6.62 s, with final errors of 0.03 bar, 0.021 bar, and 0.0065 bar for PID, PSO-PID, and CO-PID, respectively. The simulation results yielded settling times of 7.1 s, 6.1 s, and 5.9 s, with final errors of 0.04 bar, 0.033 bar, and 0.03 bar. When the pressure control results from both ports were considered together, the PSO-PID controller reduced the average settling time by 12.8% compared with the conventional PID controller, whereas CO-PID achieved a greater reduction of 16.4%. In terms of pressure accuracy, CO-PID reduced the steady-state error by 47.9% relative to PID and by an average of 37.5% compared with PSO-PID.

Overall, these results demonstrate that the CO-PID controller consistently outperforms both PSO-PID and conventional PID in terms of response speed and accuracy. The MATLAB/Simulink simulation model accurately predicts the system dynamics, and the proposed CO-PID approach achieves an effective balance between rapid response, steady-state accuracy, and system stability under maximum load conditions in both simulation and experimental evaluations. The experimental results demonstrate that the superiority of the CO-PID controller is not limited to simulation performance indicators but is clearly evident in practical applications and under less-than-ideal operating conditions. At maximum load (30 kg), the system exhibits less sensitivity to load variations, indicating higher dynamic robustness in the face of changes in inertia and hydraulic resistance. Under conditions of stress and operational uncertainty, the CO-PID controller maintained a more stable dynamic response with fewer fluctuations and a shorter settling time. Specifically, at port B and under a 30 kg load, the steady-state pressure error using CO-PID reached only 0.0065 bar, lower than the values obtained using both PSO-PID and the conventional PID controller, while also achieving a shorter settling time.

These results confirm that the CO-PID controller maintains pressure control accuracy even with increasing inertia and hydraulic resistance. Although the differences in ITAE values between CO-PID and PSO-PID in the simulation were minor, the experimental results show that CO-PID provides a significant and substantial improvement in robustness, reduced sensitivity to load variations, and overall system stability—advantages that are not fully captured by numerical performance indicators alone.

V. CONCLUSION

In this study, the design, simulation, and experimental evaluation of an electro-hydraulic elevator system were performed using MATLAB/Simulink. The system includes a hydraulic cylinder, proportional valves, pressure sensors, and a displacement sensor. A Proportional–Integral–Derivative (PID) controller was manually tuned using a trial-and-error approach. Subsequently, Particle Swarm Optimization (PSO) and Cheetah Optimizer (CO) algorithms were applied to fine-tune the PID controller parameters. The parameters of all three controllers were then fed into PID controllers integrated for displacement and pressure within a Programmable Logic Controller (PLC). The results showed that both algorithms improved system accuracy and responsiveness and reduced oscillations

compared with the conventional PID controller. The CO-PID controller outperformed the PSO-PID controller by achieving greater system stability and lower steady-state error, resulting in smoother cabin movement, more precise control, and higher reliability under varying loads. The order of the controllers was consistent with both the simulation and experimental results.

The key innovation of this research is the integration of practical implementation and modeling using MATLAB/Simulink for an electro-hydraulic elevator system, in which the pressure and displacement loops are controlled simultaneously using advanced PID controllers. This work provides a comprehensive comparison between conventional PID, PSO, and CO techniques under the same operating conditions. This contrasts with previous studies that focused on a single optimization technique, a single system variable, or simulation only. Future work may expand the system to handle more complex loads and integrate intelligent smart technologies such as neural networks or reinforcement learning for real-time control.

REFERENCES

[1] H. Yang, W. Sun, and B. Xu, "New Investigation in Energy Regeneration of Hydraulic Elevators," *IEEE/ASME Transactions on Mechatronics*, vol. 12, no. 5, pp. 519–526, Oct. 2007, https://doi.org/10.1109/TMECH.2007.905691.

[2] B. Xu, P. Dong, J. Zhang, and J. Yao, "Research on a novel flow rate inferential measurement method and its application in hydraulic elevators," *Proceedings of the Institution of Mechanical Engineers, Part C: Journal of Mechanical Engineering Science*, vol. 231, no. 2, pp. 372–386, Jan. 2017, https://doi.org/10.1177/0954406216638884.

[3] Y. Huayong, Y. Jian, and X. Bing, "Computational simulation and experimental research on speed control of VVVF hydraulic elevator," *Control Engineering Practice*, vol. 12, no. 5, pp. 563–568, May 2004, https://doi.org/10.1016/S0967-0661(03)00139-4.

[4] X. Xu and Q. Wang, "Speed control of hydraulic elevator by using PID controller and self-tuning fuzzy PID controller," in *2017 32nd Youth Academic Annual Conference of Chinese Association of Automation*, Hefei, China, 2017, pp. 812–817, https://doi.org/10.1109/YAC.2017.7967521.

[5] J. A.-K. Mohammed, W. M. Hashim, and B. S. Beram, "Speed Control of Hydraulic Elevator by Using Electro-Hydraulic Servo Mechanism," *Journal of University of Babylon for Engineering Sciences*, vol. 27, no. 4, pp. 275–291, 2019.

[6] Ł. Stawiński, A. Kosucki, A. Morawiec, and J. Skowrońska, "A new approach to controlling a hydraulic indirect elevator with a variable-speed pump," *Archives of Civil and Mechanical Engineering*, vol. 23, no. 2, Mar. 2023, Art. no. 91, https://doi.org/10.1007/s43452-023-00629-3.

[7] I. H. A. Al-Had, F. M. Mohammed, and J. A.-K. Mohammed, "Modeling and simulation of electro-hydraulic telescopic elevator system controlled by programmable logic controller," *Indonesian Journal of Electrical Engineering and Computer Science*, vol. 27, no. 1, pp. 71–78, July 2022, https://doi.org/10.11591/ijeecs.v27.i1.pp71-78.

[8] F. M. Mohammed, J. A. Mohammed, and H. S. Mohammed, "Manufacturing of Electro-hydraulic Elevator System Controlled by PLC," *Anbar Journal of Engineering Sciences*, vol. 11, no. 2, pp. 162–169, Nov. 2020, https://doi.org/10.37649/aengs.2020.171217.

[9] Z. Liu, Z. Gao, N. Yang, Y. Huo, and J. Liu, "Research of Hydraulic Drive Control System in Hydraulic Elevator Based on P-Q Valve," in *Proceedings of the 2015 International Conference on Mechanical Science and Engineering*, Qingdao, China, 2016, pp. 25–30, https://doi.org/10.2991/mse-15.2016.5.

[10] I. H. Abed Al-Hady, F. M. Mohammed, and J. A. K. Mohammed, "Modeling and Simulation of Telescopic Hydraulic for Elevating Purposes," *Engineering and Technology Journal*, vol. 40, no. 1, pp. 226–232, Jan. 2022, https://doi.org/10.30684/etj.v40i1.2253.

[11] H. Altınkaya and T. Kocakaya, "Comparison of PID Control Performances of Different PLC Series in a Hydraulic Proportional Valve System-An Experimental Setup," *Politeknik Dergisi*, vol. 27, no. 6, pp. 2389–2401, Dec. 2024, https://doi.org/10.2339/politeknik.1476181.

[12] G. Singh, A. Agarwal, R. K. Jarial, V. Agarwal, and M. Mondal, "PLC controlled elevator system," in *2013 Students Conference on Engineering and Systems*, Allahabad, India, 2013, pp. 1–5, https://doi.org/10.1109/SCES.2013.6547517.

[13] Z. Y. Ismeal and M. Y. Salloom, "A Comparison of the Performance Characteristics of Conventional and Proportional Valves Applied for Synchronizing Hydraulic Cylinders," *Engineering, Technology & Applied Science Research*, vol. 15, no. 4, pp. 24912–24923, Aug. 2025, https://doi.org/10.48084/etasr.11347.

[14] R. Kumar, P. K. Dwivedi, D. Praveen Reddy, and A. S. Das, "Design and implementation of hydraulic motor based elevator system," in *2014 IEEE 6th India International Conference on Power Electronics*, Kurukshetra, India, 2014, pp. 1–6, https://doi.org/10.1109/IICPE.2014.7115821.

[15] R. Li, J. Luo, C. Sun, and S. Liu, "Analysis of Electro-hydraulic Proportional Speed Control System on Conveyer," *Procedia Engineering*, vol. 31, pp. 1185–1193, Jan. 2012, https://doi.org/10.1016/j.proeng.2012.01.1161.

[16] J. A. Mohammed, W. M. Hashim, and B. S. Beram, "Performance Improvement of a Conventional Hydraulic Elevator by Using Electro-Hydraulic Servo Mechanism," *Engineering and Technology Journal*, vol. 38, no. 5A, pp. 748–760, May 2020, https://doi.org/10.30684/etj.v38i5A.367.

[17] M. Z. Shaikh, M. Hussain, D. Kumar, F. A. Memon, B. Rustam, and E. N. Baro, "Design and implementation of PID based flow rate control using PLC," *Mehran University Research Journal of Engineering and Technology*, vol. 42, no. 4, pp. 115–122, Oct. 2023, https://doi.org/10.22581/muet1982.2304.2515.

[18] K. Sobbouhi, F. Aghadavoudi, and M. Baharizadeh, "Implementation and Simulation of an Automated PLC Hydraulic System for a Double-acting Actuator Using a Proportional Valve," *Journal of Modern Processes in Manufacturing and Production*, vol. 11, no. 3, pp. 41–49, Nov. 2022.

[19] T. X. T. Phan, H. T. Duong, and V. Y. T. Lu, "PID-based control strategies for enhancing stability and precision in electro-hydraulic actuation systems," *International Journal of Science and Research Archive*, vol. 13, no. 1, pp. 3107–3114, Oct. 2024, https://doi.org/10.30574/ijsra.2024.13.1.2007.

[20] A. F. Ozalp, R. Polat, C. Cetinkaya, and M. H. Cetin, "Investigation of a Digital Hydraulic Valve Operated by Servo Motors," *Engineering, Technology & Applied Science Research*, vol. 11, no. 6, pp. 7957–7963, Dec. 2021, https://doi.org/10.48084/etasr.4598.

[21] W. Ma, S. Ma, W. Qiao, D. Cao, and C. Yin, "Research on PID Controller of Excavator Electro-Hydraulic System Based on Improved Differential Evolution," *Machines*, vol. 11, no. 2, Jan. 2023, Art. no. 143, https://doi.org/10.3390/machines11020143.

[22] W. M. Hashim, H. A. Al-Salihi, and F. N. A. Zubaidi, "Effects of temperature on the properties of HL32 oil in the conventional hydraulic actuators," *Heliyon*, vol. 8, no. 12, Dec. 2022, Art. no. e11831, https://doi.org/10.1016/j.heliyon.2022.e11831.

[23] A. H. Hansen, "Fluid Power Systems Design," in *Fluid Power Systems: A Lecture Note in Modelling, Analysis and Control*, Cham, Switzerland: Springer International Publishing, 2023, pp. 195–205, https://doi.org/10.1007/978-3-031-15089-0_15.

[24] T. Glück, A. Lobe, A. Trachte, M. Bitzer, and W. Kemmetmüller, "Hybrid control of hydraulic directional valves: Integrating physics-based and data-driven models for enhanced accuracy and efficiency," *ISA Transactions*, vol. 157, pp. 280–292, Feb. 2025, https://doi.org/10.1016/j.isatra.2024.12.029.

[25] Y. Li, K. H. Ang, and G. C. Y. Chong, "PID control system analysis and design," *IEEE Control Systems Magazine*, vol. 26, no. 1, pp. 32–41, Feb. 2006, https://doi.org/10.1109/MCS.2006.1580152.

[26] M. Jain, V. Saihjpal, N. Singh, and S. B. Singh, "An Overview of Variants and Advancements of PSO Algorithm," *Applied Sciences*, vol. 12, no. 17, Aug. 2022, Art. no. 8392, https://doi.org/10.3390/app12178392.

[27] M. A. Akbari, M. Zare, R. Azizipanah-abarghooee, S. Mirjalili, and M. Deriche, "The cheetah optimizer: a nature-inspired metaheuristic algorithm for large-scale optimization problems," *Scientific Reports*, vol. 12, no. 1, June 2022, Art. no. 10953, https://doi.org/10.1038/s41598-022-14338-z.